NASA/TM—2010-216241

Directivity of a Sparse Array in the Presence of Atmospheric-Induced Phase Fluctuations for Deep Space Communications

James A. Nessel and Roberto J. Acosta
Glenn Research Center, Cleveland, Ohio

March 2010

NASA STI Program . . . in Profile

Since its founding, NASA has been dedicated to the advancement of aeronautics and space science. The NASA Scientific and Technical Information (STI) program plays a key part in helping NASA maintain this important role.

The NASA STI Program operates under the auspices of the Agency Chief Information Officer. It collects, organizes, provides for archiving, and disseminates NASA's STI. The NASA STI program provides access to the NASA Aeronautics and Space Database and its public interface, the NASA Technical Reports Server, thus providing one of the largest collections of aeronautical and space science STI in the world. Results are published in both non-NASA channels and by NASA in the NASA STI Report Series, which includes the following report types:

- TECHNICAL PUBLICATION. Reports of completed research or a major significant phase of research that present the results of NASA programs and include extensive data or theoretical analysis. Includes compilations of significant scientific and technical data and information deemed to be of continuing reference value. NASA counterpart of peer-reviewed formal professional papers but has less stringent limitations on manuscript length and extent of graphic presentations.

- TECHNICAL MEMORANDUM. Scientific and technical findings that are preliminary or of specialized interest, e.g., quick release reports, working papers, and bibliographies that contain minimal annotation. Does not contain extensive analysis.

- CONTRACTOR REPORT. Scientific and technical findings by NASA-sponsored contractors and grantees.

- CONFERENCE PUBLICATION. Collected papers from scientific and technical conferences, symposia, seminars, or other meetings sponsored or cosponsored by NASA.

- SPECIAL PUBLICATION. Scientific, technical, or historical information from NASA programs, projects, and missions, often concerned with subjects having substantial public interest.

- TECHNICAL TRANSLATION. English-language translations of foreign scientific and technical material pertinent to NASA's mission.

Specialized services also include creating custom thesauri, building customized databases, organizing and publishing research results.

For more information about the NASA STI program, see the following:

- Access the NASA STI program home page at *http://www.sti.nasa.gov*

- E-mail your question via the Internet to *help@sti.nasa.gov*

- Fax your question to the NASA STI Help Desk at 443–757–5803

- Telephone the NASA STI Help Desk at 443–757–5802

- Write to:
  NASA Center for AeroSpace Information (CASI)
  7115 Standard Drive
  Hanover, MD 21076–1320

NASA/TM—2010-216241

Directivity of a Sparse Array in the Presence of Atmospheric-Induced Phase Fluctuations for Deep Space Communications

James A. Nessel and Roberto J. Acosta
Glenn Research Center, Cleveland, Ohio

National Aeronautics and
Space Administration

Glenn Research Center
Cleveland, Ohio 44135

March 2010

Level of Review: This material has been technically reviewed by technical management.

Available from

NASA Center for Aerospace Information
7115 Standard Drive
Hanover, MD 21076–1320

National Technical Information Service
5301 Shawnee Road
Alexandria, VA 22312

Available electronically at http://gltrs.grc.nasa.gov

Directivity of a Sparse Array in the Presence of Atmospheric-Induced Phase Fluctuations for Deep Space Communications

James A. Nessel and Roberto J. Acosta
National Aeronautics and Space Administration
Glenn Research Center
Cleveland, Ohio 44135

Abstract

Widely distributed (sparse) ground-based arrays have been utilized for decades in the radio science community for imaging celestial objects, but have only recently become an option for deep space communications applications with the advent of the proposed Next Generation Deep Space Network (DSN) array. But whereas in astronomical imaging, observations (receive-mode only) are made on the order of minutes to hours and atmospheric-induced aberrations can be mostly corrected for in post-processing, communications applications require transmit capabilities and real-time corrections over time scales as short as fractions of a second. This presents an unavoidable problem with the use of sparse arrays for deep space communications at Ka-band which has yet to be successfully resolved, particularly for uplink arraying. In this paper, an analysis of the performance of a sparse antenna array, in terms of its directivity, is performed to derive a closed form solution to the expected array loss in the presence of atmospheric-induced phase fluctuations. The theoretical derivation for array directivity degradation is validated with interferometric measurements for a two-element array taken at Goldstone, California. With the validity of the model established, an arbitrary 27-element array geometry is defined at Goldstone, California, to ascertain its performance in the presence of phase fluctuations. It is concluded that a combination of compact array geometry and atmospheric compensation is necessary to ensure high levels of availability.

1.0 Introduction

Widely distributed (sparse) ground-based arrays have been utilized for decades in the radio science community for imaging celestial objects and for various astrometric measurements. By correlating measurements taken by several widely separated antennas, an effective aperture area of the distance between the furthest separated antennas is created, drastically increasing the spatial resolution of the system. However, the natural "seeing" ability of a particular site will be fundamentally limited by the local atmospheric-induced phase fluctuations imposed on the signal. This phenomenon is a result of large amounts of inhomogeneous distributions of water vapor exposed to turbulent air flow conditions in Earth's upper atmosphere (troposphere), which directly leads to variations in the effective electrical path length (phase) of a received signal. Such variations are seen as 'phase noise' and will inherently degrade the resolution of radio arrays.

The same issues arise when developing sparse arrays for intrastellar communications. But whereas radio science applications impose only receive-mode requirements (i.e., imaging) and observations are made on the order of minutes to hours (long integration times), communications applications require both transmit and receive capabilities, as well as real-time corrections over time scales as short as fractions of a second. In the receive case, adaptive techniques have been utilized by the DSN since the 1980s to compensate for the atmosphere at frequencies up to X-band (Ref. 1). More recently, uplink arraying of a 7.15 GHz signal was successfully demonstrated in an experiment with the Mars Global Surveyor (Ref. 2). However, since this atmospheric phase noise scales with frequency, at Ka-band (the frequencies of interest for future NASA DSN operations) the problem becomes much more severe and has yet to be successfully resolved, particularly in the uplink. In this paper, an analysis of the performance of a sparse antenna array, in terms of its directivity, is performed to derive a closed form solution to the expected array loss in the

presence of atmospheric-induced phase fluctuations. The theoretical derivation for array directivity degradation is validated with interferometric measurements for a two-element array taken at Goldstone, California. Excellent agreement between theory and measurement is observed for the case of a two-element array. With the validity of the model established, an arbitrary 27-element array geometry is defined at Goldstone, California, to ascertain its theoretical performance in the presence of phase fluctuations.

2.0 Theory

Consider a widely distributed ($d >> \lambda$) array of N elements arbitrarily spaced on a plane, whose geometry is defined in Figure 1, where $\hat{a}_r$ is a unit vector in the direction of propagation, $\vec{\rho}_m$ is the distance from the array origin to the mth element, R is the distance the signal travels from the array origin to the receiver, and r_m is the distance the signal travels from the mth element to the receiver.

Let us assume that each element has its maximum radiation intensity in the +z direction and has zero radiation in the lower half-space ($z < 0$). Further, we will utilize the well known pattern approximation of $\cos^q(\theta)$ for the E- and H- planes of the antennas to simplify the analysis. Thus, for an arbitrarily polarized antenna element, we can represent its far field electric field, $\vec{E}_m$, in the upper half-space ($0 \le \theta \le \pi/2$) by (Ref. 3)

$$\vec{E}_m(r,\theta,\phi) = I_m\left(\frac{e^{-jkr}}{4\pi r}\right)\left[\hat{\theta}V_{Em}(\theta)\left(ae^{j\psi}\cos\phi + b\sin\phi\right) + \hat{\phi}V_{Hm}(\theta)\left(-ae^{j\psi}\sin\phi + b\cos\phi\right)\right]$$

where,

$I_m = C_m e^{j\varphi_m}$ = complex excitation coefficient

$k = 2\pi/\lambda$ = wavenumber

$V_{Em}(\theta) = \cos^{q_E}(\theta)$ = E − plane voltage pattern approximation

$V_{Hm}(\theta) = \cos^{q_H}(\theta)$ = H − plane voltage pattern approximation

(a, b, ψ) = polarization coefficients (see Table I)

TABLE I.—VARIOUS FEED POLARIZATIONS

	a	b	ψ
Linear X	1	0	0
Linear Y	0	1	0
RHCP	$1/\sqrt{2}$	$1/\sqrt{2}$	$\pi/2$
LHCP	$1/\sqrt{2}$	$1/\sqrt{2}$	$-\pi/2$

If we translate this analysis to an array environment, the array of antennas will produce a far field electric field that will consist of the superposition of each individual element field plus a propagation delay, as determined by the geometry, relative to some specified origin (see inset of Fig. 1). This will result in an array far field, $\vec{E}_{array}$, which can be represented by the product of the individual element far field and an array factor.

$$\vec{E}_{array}(r,\theta,\phi) = \overrightarrow{f(\theta,\phi)}\left(\frac{e^{-jkR}}{4\pi R}\right)\sum_{m=1}^{N} I_m e^{-jk\hat{a}_r\cdot\vec{\rho}_m}$$

where,

$\overrightarrow{f(\theta,\phi)} = \hat{\theta}V_{Em}(\theta)\left(ae^{j\psi}\cos\phi + b\sin\phi\right) + \hat{\phi}V_{Hm}(\theta)\left(-ae^{j\psi}\sin\phi + b\cos\phi\right)$

$\hat{a}_r$ = unit vector in direction of propagation

$\vec{\rho}_m$ = position vector of element relative to array origin

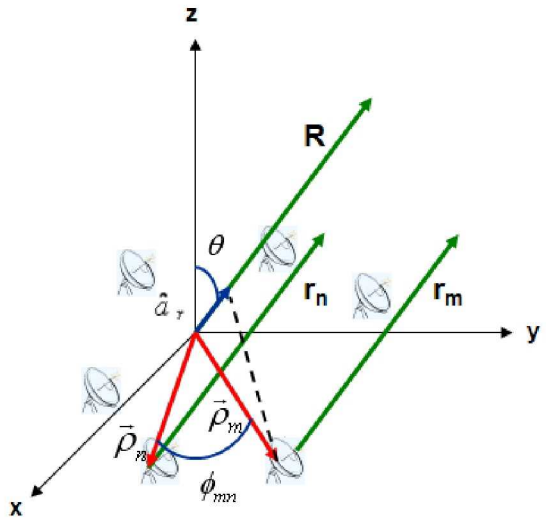

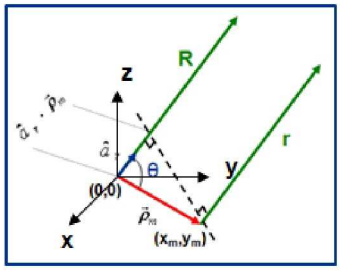

The projection of $\vec{\rho}_m$ in the direction of $\hat{a}_r$: $\hat{a}_r \cdot \vec{\rho}_m = |\vec{\rho}_m| \cos\theta$

$R = r + \hat{a}_r \cdot \vec{\rho}_m$

Figure 1.—Geometry of a planar array of radiating elements located at arbitrary positions with arbitrary polarization. Inset: determination of excess path delay between array elements as a result of array geometry.

From the far field array pattern, the radiation intensity, $U(\theta,\phi)$, and radiated power, P_{rad}, of an array can be determined, whose ratio defines the array directivity. The complete derivation of the array directivity, which involves reducing Bessel functions of 2nd order (Ref. 3), are omitted here for conciseness, but if we assume the antenna elements are identical, spaced many wavelengths apart, and there are no pointing losses to consider, then the peak directivity, D_{peak}, as a function of deterministic phase, φ, can be approximated by

Peak Radiation Intensity:

$$U\left(\theta_{peak},\phi_{peak}\right) = \frac{r^2}{2\eta}\left|\vec{E}\left(r,\theta_{peak},\phi_{peak}\right)\right|^2 = \frac{1}{32\pi^2\eta}\sum_{m=1}^{N}\sum_{n=1}^{N} e^{j(\varphi_m-\varphi_n)}$$

Radiated Power:

$$P_{rad} = \frac{1}{16\pi\eta}\left[\frac{q_E+q_H+1}{(2q_E+1)(2q_H+1)}\right]N$$

Peak Directivity:

$$D_{peak} = \frac{4\pi U\left(\theta_{peak},\phi_{peak}\right)}{P_{rad}} = D_{element}\frac{1}{N}\sum_{m=1}^{N}\sum_{n=1}^{N} e^{j(\varphi_m-\varphi_n)}$$

where,

$$D_{element} = \frac{2(2q_E+1)(2q_H+1)}{q_E+q_H+1}$$

2.1 Array Directivity in Presence of Random Phase

The above analysis assumes a constant deterministic phase between elements, but if we now suppose that random phase fluctuations are present during signal transmission, such as those induced by water vapor in the atmosphere, the statistical distribution of the random process can be utilized to obtain a closed-form solution. Let us assume (and later confirm this assumption) that the phase fluctuations induced by the atmosphere are normally distributed over the time scale of interest with mean zero and variance σ^2. The average peak directivity of an array, in terms of the statistical ensemble average of the random phase fluctuations between elements *m* and *n*, can be determined, in closed form, as

$$\langle D_{peak}\rangle = D_{element}\frac{1}{N}\sum_{m=1}^{N}\sum_{n=1}^{N}\langle e^{j(\delta_{mn})}\rangle$$
$$= D_{element}\frac{1}{N}\sum_{m=1}^{N}\sum_{n=1}^{N}\langle\cos\delta_{mn}\rangle + j\langle\sin\delta_{mn}\rangle$$
$$= D_{element}\frac{1}{N}\sum_{m=1}^{N}\sum_{n=1}^{N}\int_{-\infty}^{\infty}\cos\delta_{mn}\frac{1}{\sqrt{2\pi}\sigma_{mn}}e^{-\frac{\delta_{mn}^2}{2\sigma_{mn}^2}}d\delta$$
$$= D_{element}\frac{1}{N}\sum_{m=1}^{N}\sum_{n=1}^{N}e^{-\frac{\sigma_{mn}^2}{2}}$$

where we have defined $\delta_{mn} \equiv \varphi_m - \varphi_n$. The average array loss can then be described by the difference (in dB) of the ideal directivity and the actual directivity achieved in the presence of the phase fluctuations.

$$\langle D_{loss}\rangle = 10\log(ND_{element}) - 10\log\left(\langle D_{peak}\rangle\right)$$

For a two-element (N=2) array, the above equation simplifies to

$$\langle D_{loss}\rangle = 10\log(2) - 10\log\left(\frac{1}{2}\sum_{m=1}^{2}\sum_{n=1}^{2}e^{-\frac{\sigma_{mn}^2}{2}}\right)$$
$$= 10\log(2) - 10\log\frac{1}{2}\left(e^{-\frac{\sigma_{11}^2}{2}} + e^{-\frac{\sigma_{12}^2}{2}} + e^{-\frac{\sigma_{21}^2}{2}} + e^{-\frac{\sigma_{22}^2}{2}}\right)$$
$$= 10\log(2) - 10\log\left(1 + e^{-\frac{\sigma_{12}^2}{2}}\right)$$

3.0 Validation

The above theoretical derivation for array loss can be considered exact, so long as the original assumption that differential phase fluctuations induced by the atmosphere are zero-mean, normally distributed random variables is true. Therefore, before further analysis can proceed, we first validate this assumption by investigating the probability distribution function (PDF) of differential phase fluctuations, as measured by a two-element site test interferometer currently deployed in Goldstone, California.

The two-element interferometer developed by NASA Glenn Research Center utilizes a digital I and Q receiver which monitors an unmodulated beacon signal at 20.199 GHz from a geostationary satellite, Anik F2, with a baseline separation distance of 256 m and an elevation angle of 48.5°. A localized 10 MHz GPS-disciplined rubidium oscillator provides the reference timing for all operations and data collection. A more detailed description of the system hardware and setup can be found in (Ref. 4). The signal is sampled at 3.64 MHz with an integration time of 144 ms and recorded every second. Since our measurements limit the resolution to which we can observe phase fluctuations to time scales greater than 1 second, we must make several assumptions as to the characteristics of these fluctuations at time scales comparable to a symbol period (<< 1 sec), the time scale of interest for communications applications.

3.1 Statistics of Phase Fluctuations

A representative plot of the calibrated differential phase, as measured by our two-element interferometer, is shown in Figure 2 for September 1, 2007.[1]

[1]Note: This day was arbitrarily chosen from a set of data blocks that possessed no erroneous data points. The statistics derived from this data is representative of all data collected, thus far.

We analyze the statistics for a block of data from 02:00 to 03:00 GMT (where the atmosphere appears to be mildly turbulent) and 12:00 to 13:00 GMT (where the atmosphere appears to be calmer) at different time scales. Figure 3 shows the PDF at time scales of 1 hr, 30 min, and 10 min for each of these times. From the plot, we observe that the statistics do appear to follow a zero-mean normal distribution as we extend to shorter and shorter time periods, but notice that the rms of the phase fluctuations as we move towards shorter time scales does possess some variance. Since the rms phase is the metric by which array degradation is measured, characterizing these changes at time scales comparable to a symbol period is paramount to determining array performance for communications applications.

From this analysis, we validate that the distribution of phase fluctuations induced by the atmosphere is indeed Gaussian for time scales larger than approximately 10 min. Due to the low sampling frequency, we assume that the trend observed in the statistics for this process continue to extend to shorter time scales; that is, at time scales comparable to a symbol period, the PDF of phase fluctuations remains a zero-mean, normally distributed process. To truly verify this assumption, the sampling rate of recorded phase data would need to be increased to obtain enough information at sub-second intervals.

3.2 Two-Element Array Loss: Measurement Versus Predicted

To compare the theoretically predicted array loss with measured array loss for a two-element array, we must begin with the assumption that the phase difference induced by the atmosphere is an ergodic random process. In this way, we can take the time-averaged directivity and directly compare it to the ensemble average directivity loss determined above. From the equation for peak directivity for a two-element array,

$$D_{peak}(t) = D_{element}\frac{1}{2}\sum_{m=1}^{2}\sum_{n=1}^{2} e^{j(\varphi_m(t)-\varphi_n(t))}$$

The time-averaged directivity for a given time interval, ΔT, can be described by

$$\overline{D_{peak}} = D_{element}\frac{1}{2\Delta T}\int_{t_k}^{t_k+\Delta T}\left[2 + 2e^{j(\varphi_2(t)-\varphi_1(t))}\right]dt$$

$$= D_{element}\left[1 + \frac{1}{\Delta T}\int_{t_k}^{t_k+\Delta T} e^{j\delta_{21}(t)}dt\right]$$

where

$$\delta_{21}(t) \equiv \varphi_2(t) - \varphi_1(t).$$

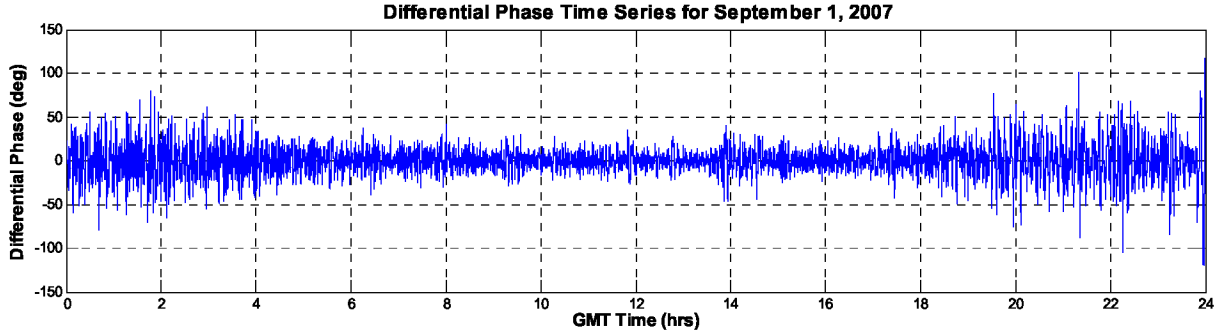

Figure 2.—Differential phase time series measured by the two-element site test interferometer at Goldstone, California, on September 1, 2007.

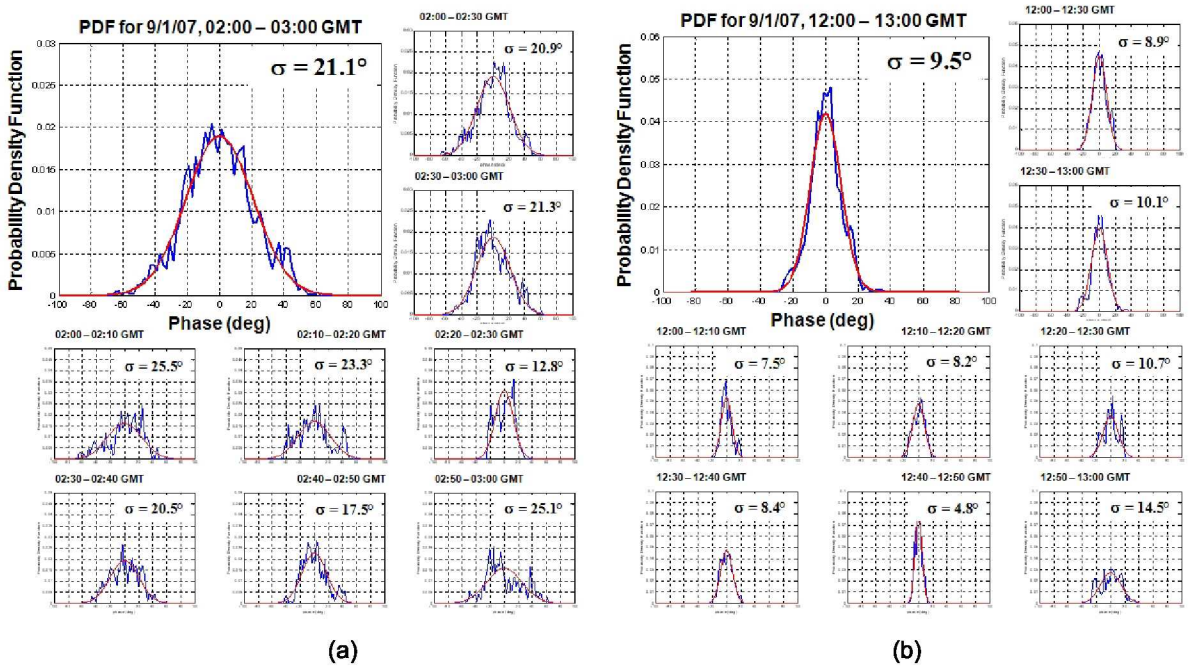

Figure 3.—PDF's of phase fluctuations for 1 hr (top left, 1), 30 min (top right, 2), and 10 min (bottom center, 6) at (a) 02:00 to 03:00 GMT and (b) 12:00 to 13:00 GMT on September 1, 2007.

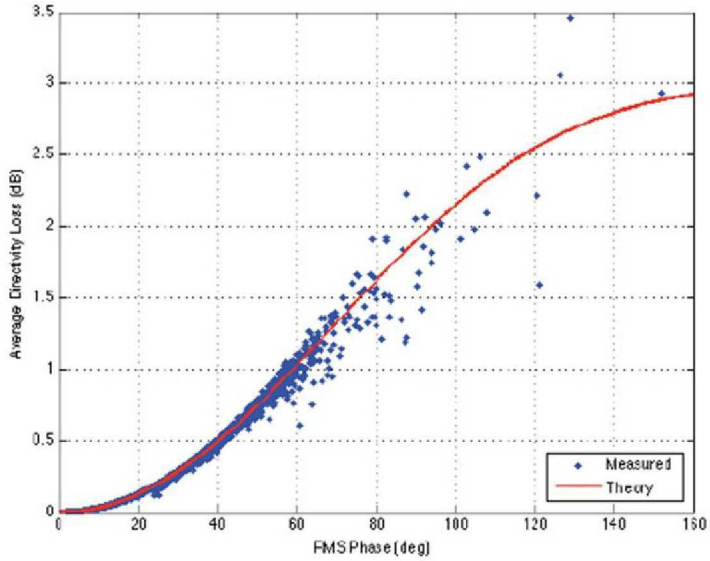

Figure 4.—Measured versus theoretical array loss for varying rms phase.

The plot of Figure 4 shows the comparison between the predicted ensemble average array degradation, $\langle D_{loss} \rangle$, for a given rms phase and the measured time-averaged directivity loss, $\overline{D_{loss}}$, for a two-element array. As 10 min is the smallest interval in which we possess enough data points to establish a normal distribution, 10 min averages were used. From the plot, we observe extremely good agreement between the two curves, indicating the correctness of the theoretical derivation for array loss in the presence of atmospheric-induced phase fluctuations, as well as confirming the ergodicity of the atmospheric-induced random process.

4.0 Typical Array Loss at Goldstone, California

To determine the typical array loss at Goldstone, California, we generate the cumulative distribution function (CDF) of the phase rms based on 1-yr data collected (2007 to 2008). To normalize our analysis, the data has been transformed to zenith and an operating frequency of 32 GHz, where the transformation to zenith is performed by multiplying by 1/air mass ($\sin(elevation\ angle)$) and the rms phase scales linearly with frequency. The baseline separation distance is 256 m. The resulting zenith rms phase CDF is shown below in Figure 5.

From the CDF, we observe that 90 percent of the time, the rms phase is better than 35.2° (at zenith), which corresponds to an array loss of only 0.39 dB (2.2 dB at 20° elevation).[2] Though this value appears low, recall that this result is for a simple two-element array. We can extrapolate this value to N elements, given a particular array geometry, by scaling the phase rms to different baselines (Ref. 5). Note that the results of this analysis will be extremely geometry dependent (Ref. 6). As a simple example, let us consider an array geometry similar to the Very Large Array (VLA) in Socorro, New Mexico, first, with an antenna spacing of 250 m between individual elements (circles in Fig. 6(a)), and one with a spacing of 50 m (x's in Fig. 6(a)). Since maximum directivity is only a function of number of elements (in widely-spaced arrays), these two geometries can be readily compared. In our analysis, we assume the theoretical Kolmogorov turbulence root phase structure function exponent of 5/6 ($d < 1$ km) and 1/3 ($d > 1$ km) to scale the phase rms to different baselines (Ref. 7). We further assume that the average rms phase between antenna elements is similar for identical baseline separations, regardless of orientation or reference. Calculating the array loss curve based on the theoretical derivation (Fig. 6(b)), we observe that for the 250-m baseline array geometry in Goldstone, California, we will need a margin of approximately 2.8 dB at zenith (12.3 dB at 20° elevation) to maintain 90 percent availability. This margin can be reduced, by reducing the baseline separation to the 50-m geometry, which only requires 1.1 dB at zenith (5.2 dB at 20° elevation). This is due entirely to the fact that small-scale fluctuations will contain much less energy than larger scale fluctuations, which would directly impact large baseline arrays. Thus, for communications applications, it will be desirable to maintain the most compact geometry possible to minimize array loss due to atmospheric phase fluctuations, as the furthest extent of the array will dominate this factor.

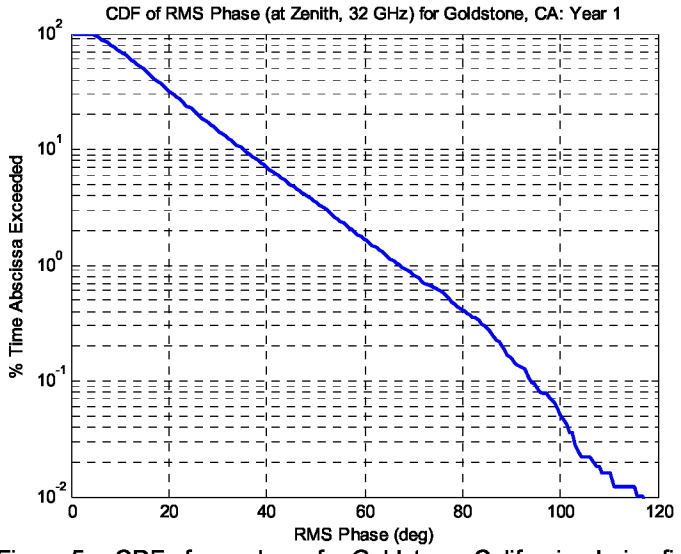

Figure 5.—CDF of rms phase for Goldstone, California, during first year of data collection.

[2]Where the air mass ($1/\sin\theta$) is used to convert rms phase at zenith to another elevation angle

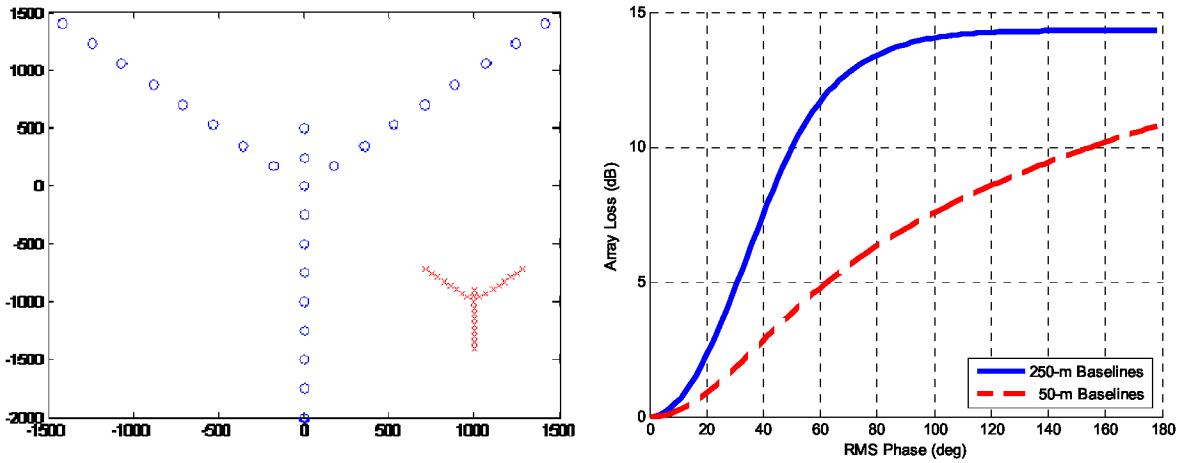

Figure 6.—(a) Model array geometries for Goldstone, California, array loss calculation example with 250-m baseline geometry (o) and a 50-m baseline geometry (x), and (b) resulting theoretical array loss versus rms phase curve.

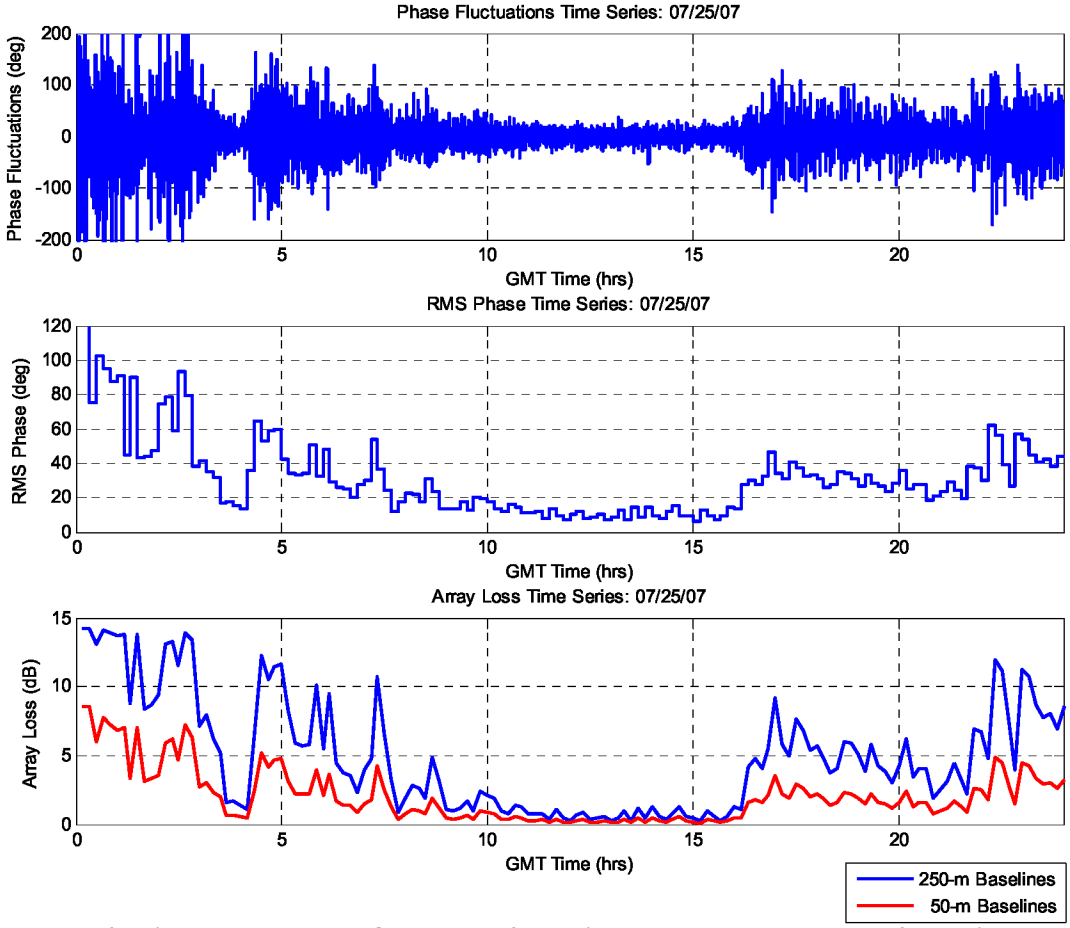

Figure 7.—(Top) Time series phase fluctuations, (middle) rms phase time series, and (bottom) calculated array loss for model arrays for July 25, 2007 measured data at Goldstone, California.

To investigate the transient behavior of the model array, we can analyze the time-domain array performance for a particularly turbulent day at Goldstone, California. Figure 7 shows the phase fluctuations observed by the two-element interferometer on July 25, 2007, as well as the resulting rms

phase and calculated array loss (for both the wide and compact array geometries described above). During extremely turbulent times (beginning of the day), array degradation can exceed 10 dB with a mean array loss of 4.4 dB for the entire day (250-m baseline geometry).[3] An approximate 2 dB improvement, on average, can be realized for the more compact array design (50-m baseline geometry).

5.0 Conclusions

Herein we report on the theoretical performance of a sparse array whose signal degradation is primarily due to atmospheric-induced phase fluctuations. The ensemble average directivity of an N element array in the presence of phase noise was derived theoretically and validated with measured data. Further, it is shown that the measured phase differential between two elements is indeed normally distributed (to the resolution limits defined by the experimental setup) and ergodic, the fundamental assumption which allows the prediction of a theoretical array's performance. It is observed that the performance of an array in the presence of atmospheric-induced phase fluctuations is limited by the furthest extent of the array elements, and, for communications applications, this geometry should remain as compact as possible. Finally, the time series performance of an arbitrary array is shown for a particularly turbulent atmospheric day. For the geometries described, there is still significant array losses observed and to prevent these losses, some form of compensation is necessary, particularly during transmit.

References

1. D. Rogstad, A. Mileant, T. Pham, *Antenna Arraying Techniques in the Deep Space Network*, John Wiley & Sons, 2003, p. 99–109.
2. V. Vilnrotter, D. Lee, T. Cornish, R. Mukai, L. Paal, "Uplink Arraying Experiment with the Mars Global Surveyor Spacecraft," IPN Progress Report 42–166, Aug. 15, 2006, p.1–14.
3. Y. Sami, S. Lee, "Directivity of Planar Array Feeds for Satellite Reflector Applications," IEEE Transaction on Antennas and Propagation, Vol. AP–31, No. 3, May 1983, p.463–470.
4. R. Acosta, B. Frantz, J. Nessel, D. Morabito, "Goldstone Site Test Interferometer", 13th Ka and Broadband Communications Conference, Turin, Italy, Sep. 24–26, 2007.
5. G. I. Taylor, The Spectrum of Turbulence, Proceedings of the Royal Society of London. Series A, Mathematical and Physical Sciences, Vol. 164, No. 919 (Feb. 18, 1938), pp. 476–490.
6. L. D'Addario, "Combining Loss of a Transmitting Array Due to Phase Errors," IPN Progress Report 42–175, Nov. 15, 2008, p.1–7.
7. C. Coulman, "Fundamental and Applied Aspects of Astronomical Seeing," Ann. Rev. Astron. Astrophys., Vol. 23, pp. 19–57, 1985.

[3]Recall that the phase data recorded at Goldstone, California, is for an elevation angle of 48.5°

REPORT DOCUMENTATION PAGE		Form Approved OMB No. 0704-0188

1. REPORT DATE *(DD-MM-YYYY)*	2. REPORT TYPE	3. DATES COVERED *(From - To)*
01-03-2010	Technical Memorandum	

4. TITLE AND SUBTITLE
Directivity of a Sparse Array in the Presence of Atmospheric-Induced Phase Fluctuations for Deep Space Communications

5a. CONTRACT NUMBER

5b. GRANT NUMBER

5c. PROGRAM ELEMENT NUMBER

6. AUTHOR(S)
Nessel, James, A.; Acosta, Roberto, J.

5d. PROJECT NUMBER

5e. TASK NUMBER

5f. WORK UNIT NUMBER
WBS 439432.04.04.07

7. PERFORMING ORGANIZATION NAME(S) AND ADDRESS(ES)
National Aeronautics and Space Administration
John H. Glenn Research Center at Lewis Field
Cleveland, Ohio 44135-3191

8. PERFORMING ORGANIZATION REPORT NUMBER
E-17228

9. SPONSORING/MONITORING AGENCY NAME(S) AND ADDRESS(ES)
National Aeronautics and Space Administration
Washington, DC 20546-0001

10. SPONSORING/MONITOR'S ACRONYM(S)
NASA

11. SPONSORING/MONITORING REPORT NUMBER
NASA/TM-2010-216241

12. DISTRIBUTION/AVAILABILITY STATEMENT
Unclassified-Unlimited
Subject Category: 32
Available electronically at http://gltrs.grc.nasa.gov
This publication is available from the NASA Center for AeroSpace Information, 443-757-5802

13. SUPPLEMENTARY NOTES

14. ABSTRACT
Widely distributed (sparse) ground-based arrays have been utilized for decades in the radio science community for imaging celestial objects, but have only recently become an option for deep space communications applications with the advent of the proposed Next Generation Deep Space Network (DSN) array. But whereas in astronomical imaging, observations (receive-mode only) are made on the order of minutes to hours and atmospheric-induced aberrations can be mostly corrected for in post-processing, communications applications require transmit capabilities and real-time corrections over time scales as short as fractions of a second. This presents an unavoidable problem with the use of sparse arrays for deep space communications at Ka-band which has yet to be successfully resolved, particularly for uplink arraying. In this paper, an analysis of the performance of a sparse antenna array, in terms of its directivity, is performed to derive a closed form solution to the expected array loss in the presence of atmospheric-induced phase fluctuations. The theoretical derivation for array directivity degradation is validated with interferometric measurements for a two-element array taken at Goldstone, California. With the validity of the model established, an arbitrary 27-element array geometry is defined at Goldstone, California, to ascertain its performance in the presence of phase fluctuations. It is concluded that a combination of compact array geometry and atmospheric compensation is necessary to ensure high levels of availability.

15. SUBJECT TERMS
Antenna arrays; Deep Space Network; Directivity; Phase noise; Atmosphere

16. SECURITY CLASSIFICATION OF:			17. LIMITATION OF ABSTRACT	18. NUMBER OF PAGES	19a. NAME OF RESPONSIBLE PERSON
a. REPORT	b. ABSTRACT	c. THIS PAGE			STI Help Desk (email:help@sti.nasa.gov)
U	U	U	UU	15	19b. TELEPHONE NUMBER *(include area code)* 443-757-5802